A Complex Convolution Kernel-Based Optical Displacement Sensor

Matthew Southwick, Zhu Mao, and Christopher Niezrecki

***Abstract*—During the last decade, a variety of optical displacement measurement techniques have been developed, commercialized and widely used. This paper presents a new type of optical displacement sensor that improves on the prior art with higher sub-pixel resolution, better accuracy, and better computation efficiency. The Complex Convolution Kernel-Based Optical Sensor (KBOS) developed in this paper leverages the phase-magnitude representation of a complex valued kernel function to achieve a superior optical displacement sensor for 2D motion measurements. The sensor's performance and properties are quantified in terms of its ability to compute the marker motions. Evaluation of this metric will explain how the sensor is able to achieve superior performance over the state of the art. The design is then validated with a set of experiments over a range of operating conditions to demonstrate the effectiveness of the approach over other existing displacement measurement techniques. Finally, the sensor's capability is compared qualitatively against other state of the art optical displacement sensors found in the literature. The sensor is shown to possess a subpixel resolution of between 1/100 and 1/2500 of a pixel depending upon spatial sampling density. The sensors dynamic range was investigated and shown to be only limited by the camera sampling speeds.**

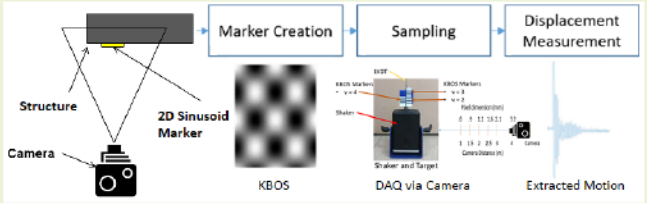

***Index Terms*—Displacement sensor, optical measurement, remote sensing, photogrammetry.**

I. Introduction

CHARACTERIZATION of structural dynamics relies upon the accurate measurement of a structure's motion in space [1]. Such measurements are commonly carried out using any number of displacement, velocity, or acceleration measurement techniques which can be broadly characterized into groups of either contact or noncontact sensors [2]. Non-contact techniques are increasingly popular as they offer the several advantages, such as not impacting the structure's mass and stiffness characteristics, requiring less instrumentation and fewer wires or data acquisition channels, enabling greater portability, and allowing for a denser set of measurement points [3]–[5].

A smaller subset of the noncontact sensor so far developed are vision based target tracking sensors which use a target affixed to the structure of interest and pattern matching algorithms to measure the targets displacements [6]–[13]. These sensors possess varied degrees of sophistication. Ji and Zhang used corner detection of a target for motion measurement [12]. Ribeiro *et al.* used a precision designed target that incorporates circle finding and corner detection to improve displacement measurements [11]. Busca *et al.* used a target designed with circles, known locations and a random pattern to perform digital image correlation with a target [13]. Such sensors suffer from a number of performance shortcomings. First, such sensors have low subpixel resolution which results in a requirement for large (poorly localized) measurement areas or poor noise floor [2], [6]–[8]. Also, this class of sensors requires the computation of highly up-sampled normalized cross-correlations for each displacement measurement which leads to slow computation speeds [2], [14]. To improve on these deficiencies, a modified Taylor Expansion interpolation approach has been used to improve the subpixel resolution and speed of the pattern matching technique [15]. Another target based lateral displacement sensor uses an optical fiber bundle and a grating with periodically varying refractive index to measure motions [16].

In addition to target based displacement sensors, non-target sensors have been developed that perform image registration on natural features of a structure to obtain displacements at the location of the tracked feature. M.Q. Feng *et al.* present a non-target sensor that allows structural displacements to be

Manuscript received February 22, 2020; accepted March 24, 2020. Date of publication April 7, 2020; date of current version August 5, 2020. This work was supported by the National Science Foundation under Grant 1762809. The associate editor coordinating the review of this article and approving it for publication was Prof. Okyay Kaynak. *(Corresponding author: Zhu Mao.)*

The authors are with the Department of Mechanical Engineering, University of Massachusetts Lowell, Lowell, MA 01854 USA (e-mail: matthew_southwick@student.uml.edu; zhu_mao@uml.edu; christopher_niezrecki@uml.edu).

Digital Object Identifier 10.1109/JSEN.2020.2986240

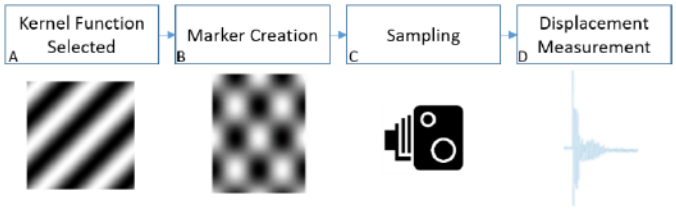

Fig. 1. Sensor application flow: marker design, instrumentation, data acquisition, and displacement calculation.

measured without needing to instrument the structure [17]. Also, Wahadwa *et al.* showed how motion magnification and edge detection can be combined to perform non-target subpixel motion measurements [18].

In this research, a novel design for a vision-based target tracking sensors is presented. This sensor uses a complex convolution kernel based target design that leverages the phase-magnitude representation of the kernel function to achieve excellent sub-pixel resolution and computation speed compared with similarly employed sensors, while maintaining excellent measurement accuracy. A controlled series of tests were carried out to evaluate the sensor's performance and the accuracy and resolution are shown to be independent of the camera orientation relative to the target.

II. The Complex Convolution Kernel-Based Optical Sensor (KBOS)

The developed sensor uses the phase-magnitude representation of a complex 2D kernel function to compute the displacements of a target present in a video frame. The sensor itself is the magnitude of the selected kernel function printed onto a sheet of adhesive paper (i.e. sticker). The sensor is sampled in space using a camera and a discrete representation of the sensor is captured. Using the sampled sensor, the orientation and scale of the target are determined by derivative optimization of the discrete convolution between the sampled space and the complex kernel function. Once the scale and orientation are known, a simple complex 2D convolution (of the same pixel size as the sampled target) is computed and results in a phase shift which is directly proportional to the designed target's known scale. From this, the target's 2D motion can be measured.

Figure 1 presents an overview of the steps performed to measure displacements with the KBOS sensor. The details of each step and its function will be explained and elaborated upon in the subsequent section.

A. Kernel Function Selection

In the development of the sensor, first the kernel function (w) must be selected. The constraints placed on the kernel function are that it must be self-orthogonal with respect to orientation and spatial shift, be complex, be periodic, and self-orthogonal at varying scales [19]. These constraints define a complex valued kernel w_c which is a quadrature pair composed of w_r the real component of the kernel and w_i the imaginary component of the kernel (1), representable through a phase-magnitude relation [20].

$$w_c = w_r + i\,w_i \tag{1}$$

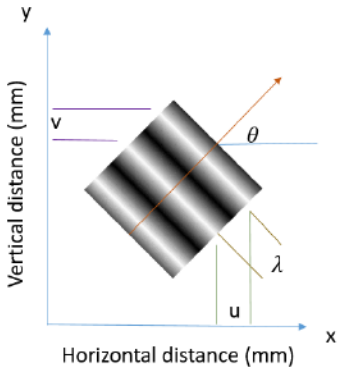

Fig. 2. Physical space manifestation of kernel function as used for the optical target.

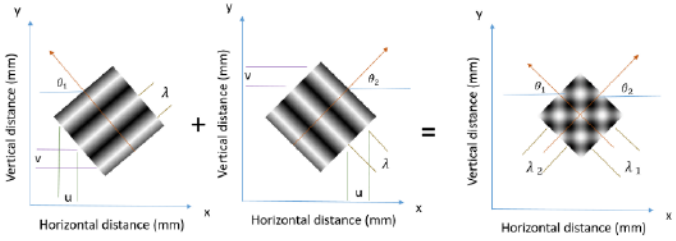

Fig. 3. 2D target derived from the superposition of two steerable 1D kernels.

These requirements ensure that by sampling the magnitude of the function as it is printed on the marker, orientation, scale and phase can all be determined with reference to the camera sampling space. The simplest function fulfilling these requirements is the complex exponential function

$$w_c = e^{-2\pi i(ux+vy)} \tag{2}$$

In (2), u and v denote the horizontal and vertical scale respectively. This function will later be used to test the KBOS technique.

B. Physical Marker Creation

As mentioned in Section II-*A*, once the kernel function is selected, a target can be generated. For a 1D test, the magnitude of the kernel function is printed out with physical dimensions customized by the user.

These physical dimensions give the kernel a scale (λ) in real space measurable in units of distance (e.g. mm) (see Fig 2).

For a 2D test, the magnitude of the linear combination of the kernel function and its 90°-rotated twin are printed out. These two functions form the basis of a 2D-space are defined by the plane of the target [21] (see Fig. 3).

C. Sampling

The markers illustrated in Fig. 2 and 3 may be sampled by means of a video camera whereby pixels perform a spatial averaging operation (see Fig. 4) of the marker to discretize it in camera memory [22]. Figure 4 shows how the pixel sampling operation performs spatial averaging to approximate a surface. Sampling of the marker produces a discrete function $f(m,n)$ that is the representation of the physical marker in the

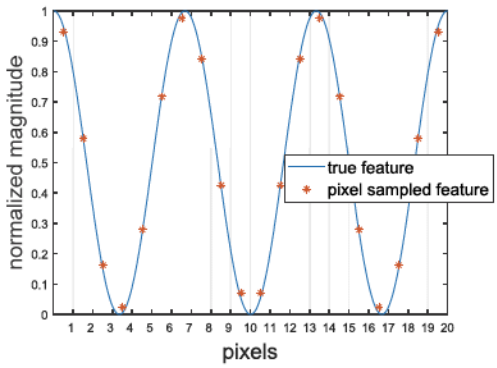

Fig. 4. Quantization error due to spatial averaging of pixel sampling.

sampling space, where m and n are the sample indices in camera space, and $0<m<M$, $0<n<N$ with M and N are the total number of samples in a given spatial direction.

To counter quantization errors produced by the sampling operation, a kernel function can be selected that mostly varies linearly so that the averaging operation places points on the function. Also, it is necessary that the target function satisfies the Nyquist sampling criterion so that information is not lost due to aliasing.

D. Displacement Measurement

With the marker sampled over time, the calculation of its 2D motions is thereby possible, which is done by using a three-step process. First, the scale of each of the independent discretized kernel functions is determined with reference to the sampling space. Next, the phase of each of the independent kernel functions is calculated. Finally, the phase is scaled by the known physical dimensions of the printed marker to obtain the true displacements of each function

1) Scale and Orientation Calculation: The scale of the discretized kernel function is calculated with high accuracy by performing gradient descent on the convolution between w_c *and f,* to find the scale parameters that maximize the wavelet transform of the initial kernel function and the sampled marker in the first frame of measurement. This operation is presented as (3).

$$0 = \nabla w_c\,(m,n) * f\,(m,n)\,, \quad 0 < m < M, 0 < n < N \tag{3}$$

The values of m and n that satisfy (3) are defined as u_0 and v_0 respectively. u_0 and v_0 then define the spacial scale of w_c to match the scale of *f, and* $w_c(u_0, v_0)$ is a spatially shifted version of *f.* The gradient descent operation returns the scale of the marker in the dimensions of the sampling space and is used to make the calculation of phase efficient, as once scale is known, only a single bin of the wavelet transform need be calculated to obtain phase.

From scale, the orientation θ of the target kernel is determined relative the camera reference frame by (4).

$$\theta = \tan^{-1}\frac{v_0}{u_0} \tag{4}$$

Thus, phase motions represent a projection of total 2D motions onto the orientation direction of the sampled function.

2) Phase Calculation: With scale of the sampled marker determined, the phase shifts of the physical marker kernel are determined frame by frame through a complex 2D convolution.

$$F = w_c(u_0, v_0) * f(m,n) \tag{5}$$

This operation does not require up-sampling in the calculation of each frame's convolution and still return a subpixel representation of motion, thus offering a dramatic improvement in calculation speed over subpixel cross correlation techniques.

Importantly, the calculation offers a very accurate measure of phase as long as the scale parameters of w_c are calculated accurately [23]. With sampling errors, the accuracy of this calculation is diminished, but will be shown through real world testing to still offer excellent accuracy. The reason for such high accuracy is primarily that for a stationary signal, this calculation is exact, and due to the weighted averaging performed by the convolution operation any stochastic noise has little effect on the calculation for sufficient measurement points ($M*N$).

3) Displacement Calculation: The final step of measuring displacements through the KBOS method is to scale the phase φ to the real world units of the target. Scaling is performed using the already known target kernel scale λ and (6).

$$x = \frac{\lambda\varphi}{2\pi} \tag{6}$$

For the 1D case the calculated displacement represents the projection of the total displacement onto the orientation direction of the sampled marker. For the 2D case, the displacements measured independently for each of the orthogonal functions allows for a calculation of the total displacement projected onto the plane of the target by (8) and (8). In (8) and (8) w_1 and φ_1 are wavelength and phase of the function with orientation θ_1 as denoted in figure 3, and w_2 and φ_2 are wavelength and phase of the function with orientation θ_2 as denoted in figure 3.

$$x = \frac{w_1\varphi_1}{2\pi}\cos\theta_1 + \frac{w_2\varphi_2}{2\pi}\sin\theta_2 \tag{7}$$

$$y = \frac{w_1\varphi_1}{2\pi}\sin\theta_1 + \frac{w_2\varphi_2}{2\pi}\cos\theta_2 \tag{8}$$

4) Camera Orientation Analysis: For all other known optical planar displacement sensors, the displacement measurement is dependent on the relative orientation of the camera to the target [2]. However, for the KBOS, the camera orientation should play no role in the calculation of the planar displacements. Therefore, although a camera rotation will cause relative lengths to change, in the camera's view, this will not affect the displacement measured. Since the phase is not affected by this projection, and the phase is rescaled by an already known wavelength, the planar displacements can therefore be measured accurately independent of the camera orientation.

III. Implementation and Validation

The effectiveness of the KBOS technique was evaluated through a series of experiments to identify measurement resolution, accuracy, and range of use.

First, a validation test was designed using a mechanical shaker to provide controlled 1D vertical motion attached to

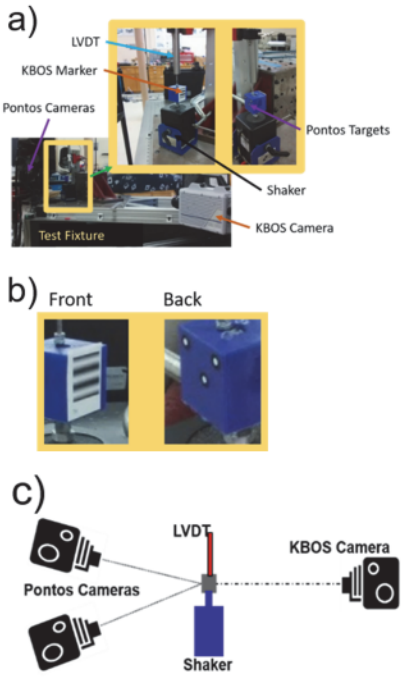

Fig. 5. a) Validation test setup using a LVDT, Point tracking system (PONTOS), and the developed KBOS system. b) Close up of the KBOS marker placed on the front of the plastic block and Pontos targets co-located on the back of the block. c) Schematic of test setup for easier visualization.

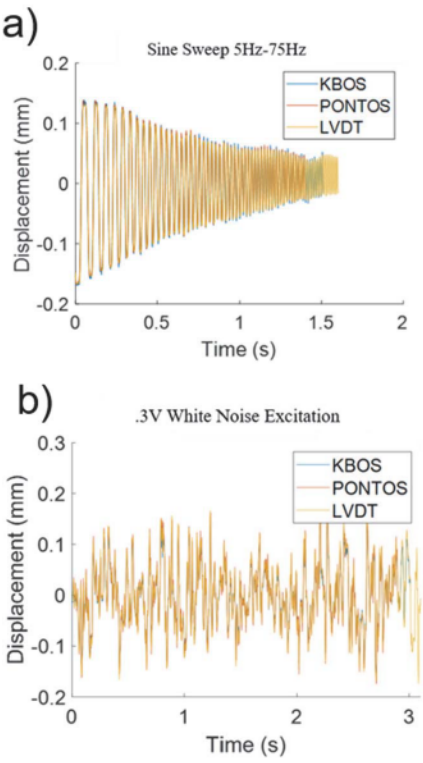

Fig. 6. a) Comparison of measured response between KBOS, LVDT, and Pontos systems for a sine sweep shaker excitation varying from 5 to 75Hz; b) Comparison of measured response between KBOS, LVDT, and Pontos systems for a white noise shaker excitation.

a rigid plastic block. This block was then instrumented with a KBOS sensor attached to its front face, a Linear Variable Differential Transformer (LVDT) attached to the top of the plastic block, and an optical target used in conjunction with an optical point tracking system (PONTOS). The LVDT and commercial point tracking system serve as a benchmark, against which the KBOS system is compared for accuracy. The validation test setup used is shown in Fig. 5.

This test setup was used in three tests that are intended to demonstrate the effectiveness of the developed sensing technique. **First,** the KBOS sensors accuracy was evaluated for broadband excitation by supplying the shaker with a variety of wave forms and simultaneously measuring displacements with the different sensors. **Second,** the sensors accuracy was evaluated at the limits of the sensor pixel span by performing tests that had progressively increasing camera distance. **Finally,** the independence to camera orientation of the developed sensor was evaluated with a test in which camera orientation relative to the target was varied. These tests all seek to evaluate the effectiveness and limitations of the sensor laid out in this work.

To evaluate the performance of the KBOS system compared to the LVDT, three important characteristics are investigated. First, the Average Error as defined in Equation 9 is used to evaluate the accuracy between the baseline LVDT (y_1) and the KBOS sensor measurement (y_2).

$$Avg.Error = |mean\,||y_1| - |y_2|\,|| \tag{9}$$

Second, the time response assurance criterion (TRAC) as defined in Equation 10 is used to evaluate the scale independent similarity between the baseline signal and KBOS measurement.

$$TRAC = \frac{\left(\sum y_1 y_2\right)^2}{\sum y_1^2 \sum y_2^2} \tag{10}$$

Third, the noise floor is defined to be five standard deviations beyond the mean of the noise signal (y_{noise}), as measured away from any harmonics present in each test. Equation 11 defines the noise floor.

$$NoiseFloor = avg\,(y_{noise}) + 5std(y_{noise}) \tag{11}$$

A. Broadband Excitation Accuracy Testing

Using the test setup shown in Fig. 5, the accuracy of the KBOS sensor was evaluated for broadband excitation. The measurement of two such broadband signals is shown in Fig. 6. In this figures, it can be seen that the measurement using the KBOS sensor is virtually identical from the baseline measurements, and the KBOS sensor has no frequency dependence when the camera frame rate is sufficient to satisfy the Nyquist criterion for the motion of interest.

Statistical comparison between the KBOS sensor and the benchmark techniques was carried out using the TRAC (Tables I and II) and the mean displacement error (Table III).

The noise floor of this test setup was also investigated for the KBOS system by taking a baseline measurement where no excitation was supplied to the shaker. The frequency domain plot (figure 7) of this baseline test offers a number of insights

TABLE I
TRAC VALUES FOR WHITE NOISE EXCITATION

	KBOS	LVDT	Pontos
KBOS	1	.915	.964
LVDT	.915	1	.952
Pontos	.964	.952	1

TABLE II
TRAC VALUES FOR SINE SWEEP EXCITATION

	KBOS	LVDT	Pontos
KBOS	1	.986	.993
LVDT	.986	1	.997
Pontos	.993	.997	1

The TRAC values presented in Table 2 are all close to one, indicating excellent correlations between the signals acquired from different sensing modalities.

TABLE III
AVERAGE ERROR FOR BOTH TESTS

	KBOS-Pontos	KBOS-LVDT	Pontos-LVDT
WHITE NOISE EXCITATION	13.6	10.2	10.3
SINE SWEEP EXCITATION	5.8	8.2	4.2

Low average displacement error shows good magnitude accuracy

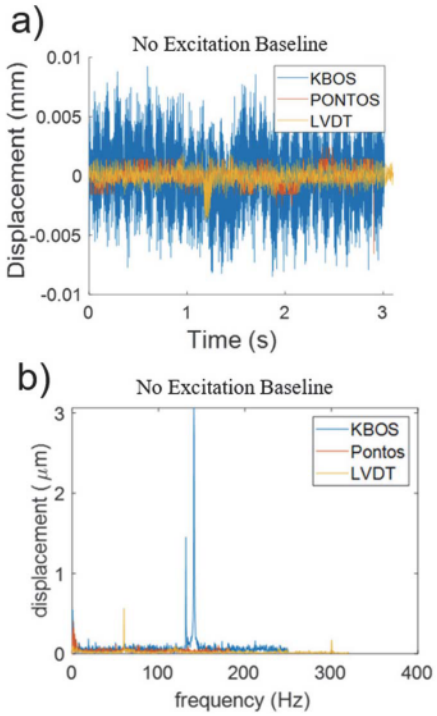

Fig. 7. a) Comparison of measured response between KBOS, LVDT, and Pontos systems with no shaker excitation; b) Comparison of measured response between KBOS, LVDT, and Pontos systems with no shaker excitation in the frequency domain. The displacement peaks that are measured by the KBOS sensor at 120Hz and 130Hz appear due to camera motion driven by the camera's cooling fan. The displacements measured by the LVDT show a peak at 60Hz due to noise from its power supply.

into the performance of the sensor. From the baseline test frequency domain data, the noise floor is calculated using Eq. 11 to be 0.184μm which is equivalent to 1/2500 of a pixel in the test.

This test represents essentially an ideal testing scenario with a controlled environment and a large marker with 55 pixels spanning an edge. The printed area chosen represents a fairly reasonable target size for use in real world testing, however, many larger scale tests may require a larger target.

B. Minimum Spatial Resolution Test

To investigate the system's measurement performance outside of an ideal envelope, where the sensor target is spanned by very few pixels as well as when the Nyquist limit of the target is exceeded, a series of tests were performed using a smaller target and progressively moving the camera further away from the target, using the test setup shown in Fig. 5. Figure 8 depicts the test series and the distances between camera and shaker used, as well as the approximate dimensions of a pixel on the KBOS marker at each camera distance.

For this test, a number of targets of varied wavelength kernel design were mounted onto the shaker and the motion of each was compared against the LVDT to determine the accuracy of the system under non-ideal measurement conditions. The shaker was supplied with a 25Hz tonal excitation providing approximately 0.03 mm peak-to-peak displacement of the shaker. Figure 9 shows examples of the displacements

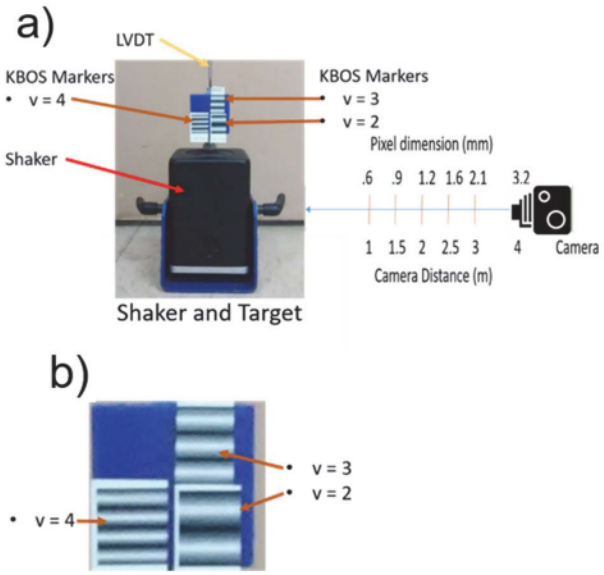

Fig. 8. a) Camera distances and associated pixel dimensions used in minimum resolution test. Shaker setup with the three different wavelength targets used in the tests. In the diagram, marker wavenumber is denoted in 1/inches by v. b) Close up of the markers used in the test.

recorded using the LVDT and KBOS sensor during the test series.

From the recorded series of tests, TRAC, Avg. Error, and noise floor values were calculated for each test to evaluate

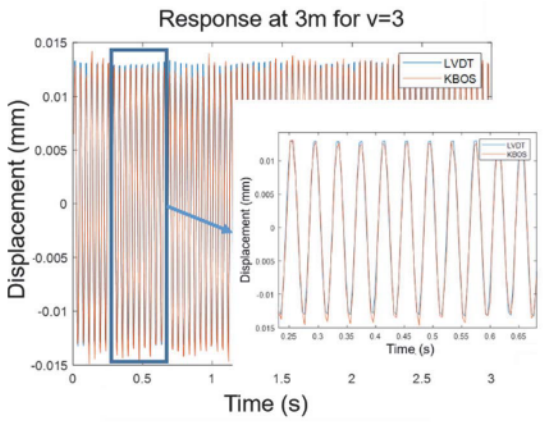

Fig. 9. Response of LVDT and KBOS for a camera distance of 3m and the target with wavenumber v=3 (1/inches). This response is representative of the responses measured for the other markers and at the varied camera distances used during the test.

the accuracy and minimum resolution of the measurement technique as target sample dimensions are diminished. Figure 10 a, b, c presents these statistics for this sequence of tests performed.

Due to the diminishing pixel dimensions of the marker as the camera distance increases, it is expected that the noise floor gradually increases as the camera distance increases which was observed. From the Avg. Error it can be noted that the accuracy of the KBOS sensor seems to be bounded by the noise floor and therefore can be said to be accurately measuring the motion of the shaker within the bounds of the noise variance. It is also noteworthy that the accuracy of the technique was independent of the wavenumber used in the target design.

C. Orientation Dependence Test

Next, a series of tests were performed to prove that the sensor accuracy is independent of the camera orientation relative to the target. This was done by using a test setup where the orientation angle of the camera was varied while the shaker motion was measured. For this test, as before, a 25Hz tone was supplied to the shaker producing a motion of approximately 0.03mm peak-to-peak. Figure 11 shows the test setup used for the orientation dependence test and define the independent angle variables (θ, Φ).

Two sets of tests were run with this setup. **First,** only the elevation angle (Φ) was varied while θ remained fixed at 0°. For this test TRAC, Avg. Error, and noise floor values were calculated for each test to evaluate the accuracy of the measurement technique as target sample dimensions are diminished. Figure 12 a, b, c presents these statistics for this sequence of tests performed.

The analysis indicates that the accuracy of the measurement is not influenced by varying the camera orientation angle, thus supporting the claim of independence to camera orientation. **Next,** a second test was run where the elevation angle Φ was held at 40° and the angle θ was varied. Figure 13 a, b, and c present the results and statistical analysis of this series of tests.

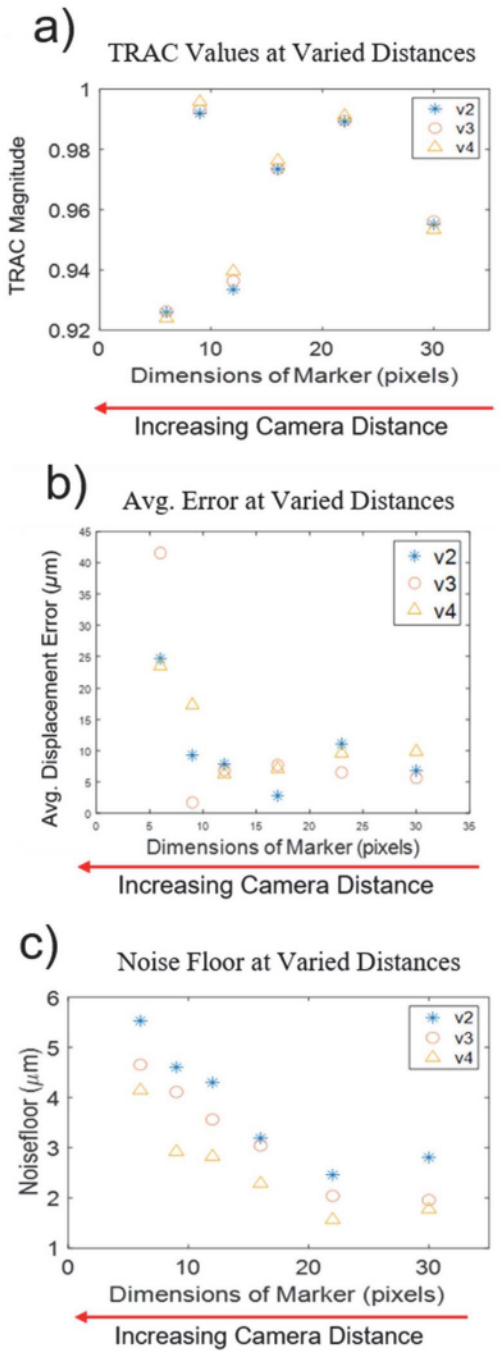

Fig. 10. a) TRAC values between the LVDT and KBOS for each marker at varied camera distances; b) Average displacement error between LVDT and KBOS for each marker at varied camera distances; c) Noise floor for KBOS at varied camera distances.

The results from both test sequences demonstrate the low sensitivity of the KBOS system measurement to angular orientation of the camera. This is a useful property because in many testing situations, it may be difficult to make measurements with the camera oriented with a normal line of sight relative to the device under test. This allows the technique to be used in a wider range of test scenarios improving its applicability and eliminating a common source of error in optical measurements.

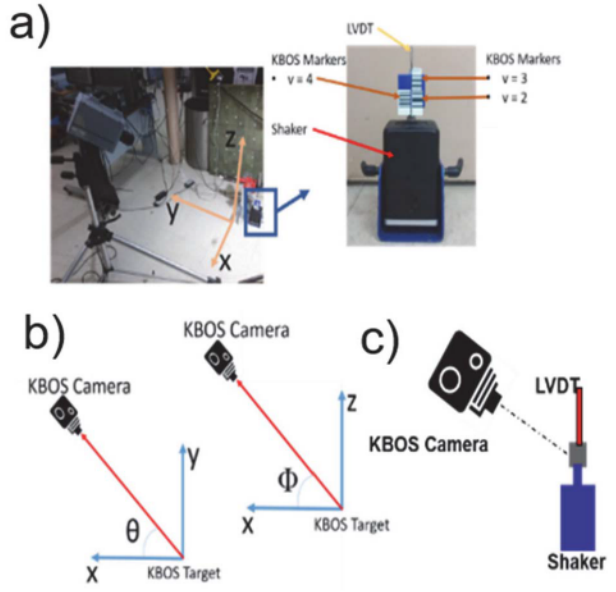

Fig. 11. a) Test setup for orientation dependence test; b) Definition of camera orientations relative to targets. c) schematic of setup for easier visualization.

IV. Comparison With the State of the Art in Optical Displacement Sensors

Target and calibration-based optical displacement techniques have allowed for the accurate non-contact motion measurements. The state of the art in this area is spanned by three well-developed techniques. First, point tracking and DIC techniques using a calibrated stereo camera system have been proven as effective techniques for making non-contact displacement measurements via optical targets and a pattern applied to a structure, respectively [3]. Second, feature based target tracking techniques using designed targets with known features have been used successfully to measure structural motions [8]. Third, area-based target tracking techniques using pattern matching have been developed to measure structural motions [2]. The KBOS system developed in this paper provides a fourth option to perform remote optical displacement measurements. The advantages and disadvantages of each system will be considered to assess the utility of the developed KBOS sensor. Figure 14 shows examples of each of the different sensors that are presented in the following sub-sections A, B, C, and D.

A. Calibration-Based Motion Measurements

Calibration-based optical displacement measurement techniques have advanced to a level where they are commercially available and have well known accuracy. The largest advantage of these techniques is that by calibrating a volume using two cameras (i.e. stereophotogrammetry), the system can measure 3D motions [3]. The technique is accurate down to its noise floor, which for a good calibration can be less than 1/1000 of a pixel [1]. The principle disadvantage of this technique is that to be accurate, it requires an extensive calibration procedure. This can be time consuming and difficult to perform when a target is far from the cameras or if the structure is large. Also,

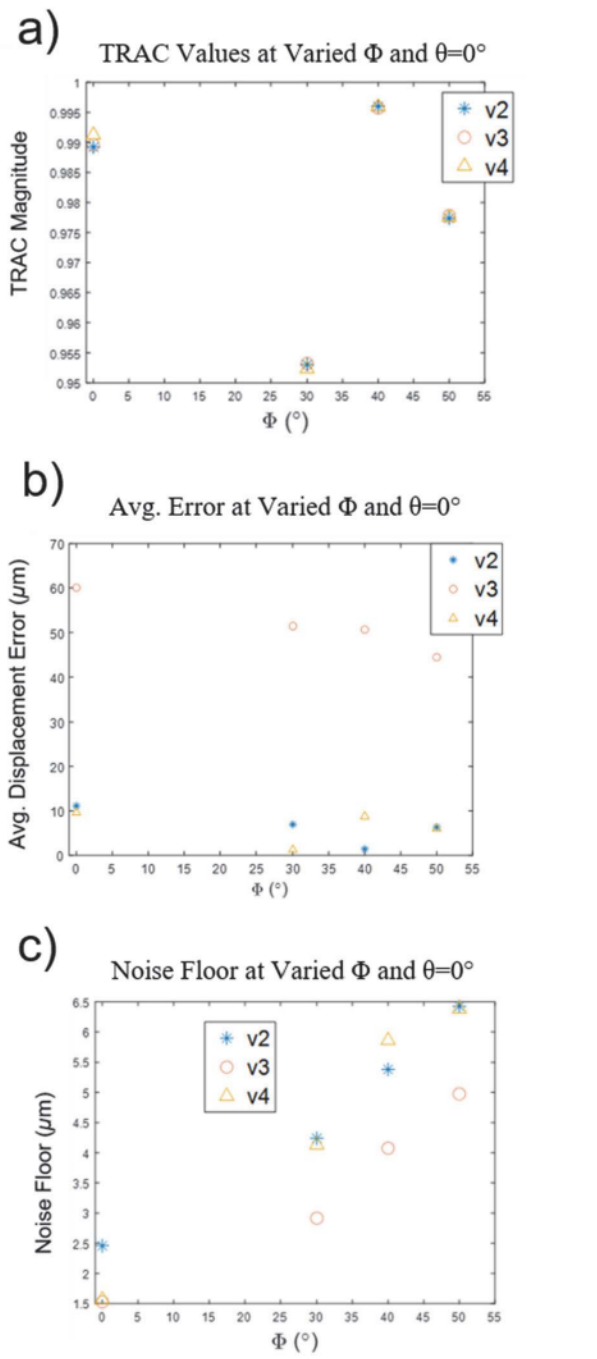

Fig. 12. a) TRAC values between LVDT and KBOS for each marker at varied angles of 8; b) Average displacement error between LVDT and KBOS for each marker at varied angles of 8; c) Noise Floor for KBOS at varied angles of 8.

because the calibration needs to be extremely precise, once calibrated, cameras cannot be moved relative to each other without disrupting the calibration [24]. Overall, the technique is effective but can be inflexible and time consuming for some types of measurements.

B. Feature-Based Target-Tracking Sensor

Feature-Based Target-Tracking Sensors are a simple approach to the design of an optical target-based displacement

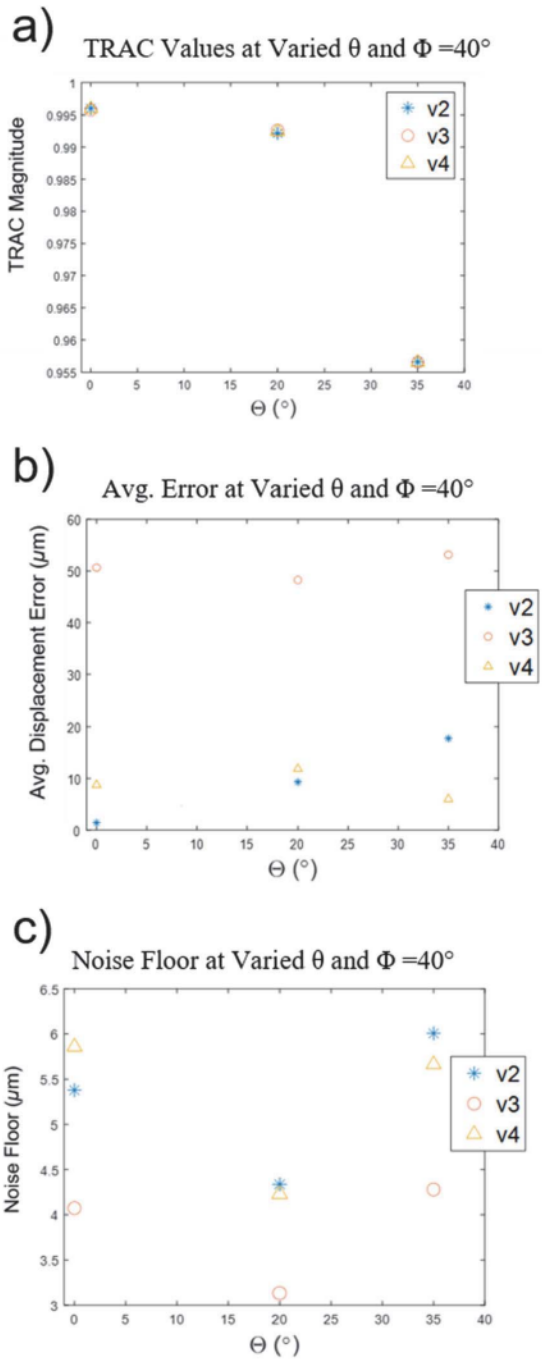

Fig. 13. a) TRAC values between LVDT and KBOS for each marker at varied angles of θ; b) Average displacement error between LVDT and KBOS for each marker at varied angles of θ; c) Noise Floor for KBOS at varied angles of θ.

sensor. These sensors use a designed pattern such as the square pattern of circles used in the work by Fukuda *et al.* [8]. This technique has been shown to be an effective approach to measuring 2D displacements remotely. The advantage of this approach is that it offers a low-cost sensor that can easily be instrumented on a structure [8]. Also, this approach is extremely computationally efficient leading to its ability as a real-time monitoring approach [8]. Unfortunately, the approach offers poor subpixel resolution and requires the use of a zoom

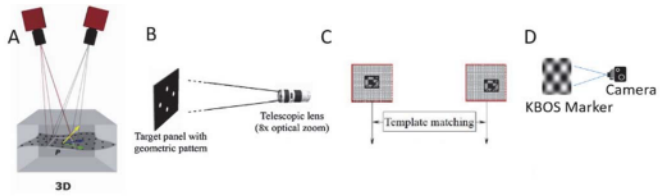

Fig. 14. a) Calibration-Based Motion Measurements [3]. b) Feature Based Target-Tracking Sensor [8]. c) Area-Based Template-Matching Sensor [9]. d) KBOS System.

lens to achieve sufficient resolution for structural motion measurements. This leads to the necessity for either large target areas with poor localization, or limited fields of view which only allows the use of a single target per camera. Overall, this technique is viable for measuring structural displacements but has its effectiveness limited by poor resolution.

C. Area-Based Template-Matching Sensor

Area-Based Template-Matching Sensors have been developed using pattern matching and phase correlation to track subpixel motions of a designed target [9]. This approach has been proven by Fukuda *et al.* for the measurement of civil structure motions [10]. The approach improves on feature-based target-tracking by using the entire area of a target to measure displacements thus improving the resolution of the measurement [2]. The approach is accurate and effective but suffers from a number of drawbacks. First, the subpixel resolution of the approach is limited compared to calibration-based techniques only achieving less than 1/20 of a pixel due to systematic errors in the phase correlation approach and measurement system which limit the max achievable resolution [9]. Also, the system has a dependence on the orientation between the camera and target. For a non-perpendicular target, the measurement is off by a factor dependent on the angle of the camera and thereby decreases accuracy of the measurement system in many real world test situations [9]. Additionally, measurement of the sensor's orientation is limited in resolution due to limits on the amount of information that can be encoded in the sensor's pattern [7]. Finally, a highly up-sampled cross correlation becomes a computationally expensive process as the discrete Fourier transform (DFT) of a large image must be computed. This limits the real time applicability of the approach to using 150-fps sampling to achieve real-time results [9]. Overall, the approach is an effective method for cheaply measuring 2D structural motions but is not the most accurate or high resolution approach available.

D. KBOS System

The KBOS system developed in this paper uses a phase-based approach to motion measurement to achieve 1D displacement measurements of a target printed with a designed pattern. In this work, it has been shown that the KBOS sensor is an accurate approach to displacement measurements down to the accuracy limited by the noise floor of the KBOS system. This noise floor has been shown to be less than 1/1000 of a pixel for a sufficiently sampled target (~50 pixels per edge)

and remains better than 1/100 of a pixel even down to the sampling approaching the Nyquist limit of the target. The approach also is extremely computationally efficient, achieving better than 0.5 milliseconds per frame after the first frame has been calculated. This could allow for high frame rate real time monitoring using the approach. Also, the technique has been shown to be independent on camera orientation relative to the target, which allows for better flexibility in test setup and feasibility for a variety of applications. Overall, the KBOS approach offers improvements with some combination of resolution, speed, and flexibility over each of the state-of–the-art systems described, making it an improved optical displacement sensor that is applicable to any situation where the previously described 2D motion measurement approaches have found success.

V. Conclusion

In this work, a new optical displacement sensor has been developed in the form of the KBOS system. The design of this sensor has been laid out and its properties described. It has also been shown to be an effective technique working with high subpixel resolution over small sampling areas. This allows the sensor to be made small for localization or allows for large fields of view which could include multiple sensors. Next, the sensors independence on relative orientation between camera and target has been demonstrated to illustrate the sensors flexibility, requiring only line of sight and acceptable sampling to achieve accurate displacement measurements. The testing and analysis of the sensor showed that the KBOS sensor can achieve between 1/2500 and 1/100 pixel resolution dependent upon spatial sampling density. The sensor was also shown to be able to capture any dynamic range up to the sampling limits of the camera. The KBOS sensor is expected to be a versatile tool for the measurement of the motions of structures, improving on other 2D motion measurement techniques in its measurement performance.

In the future, the properties of this sensor will be investigated in further detail, with the goal of developing an analytical uncertainty quantification framework for the sensor to improve its effectiveness and implementation. Also, the sensor's performance in real world scenarios will be evaluated, using the developed sensor to perform non-contact assessment on a real structure outside of the lab. Finally, work is underway to develop the sensor from a 2D approach to a 3D technique using a stereo set of cameras. The goal of this is to produce a calibration-free 3D optical displacement sensor with accuracy and resolution on par with commercially available calibration-based optical measurement techniques.

Acknowledgment

This work is supported by the National Science Foundation under Grant No. 1762809. Any opinions, findings, and conclusions or recommendations expressed in this material are those of the authors and do not necessarily reflect the views of the National Science Foundation.

References

[1] P. Kohut *et al.*, "Monitoring of a civil structure's state based on noncontact measurements," *Struct. Health Monit., Int. J.*, vol. 12, nos. 5–6, pp. 411–429, Sep. 2013.

[2] D. Feng and M. Q. Feng, "Computer vision for SHM of civil infrastructure: From dynamic response measurement to damage detection—A review," *Eng. Struct.*, vol. 156, pp. 105–117, Feb. 2018.

[3] M. N. Helfrick, C. Niezrecki, P. Avitabile, and T. Schmidt, "3D digital image correlation methods for full-field vibration measurement," *Mech. Syst. Signal Process.*, vol. 25, no. 3, pp. 917–927, Apr. 2011.

[4] L. Yu and B. Pan, "Full-frame, high-speed 3D shape and deformation measurements using stereo-digital image correlation and a single color high-speed camera," *Opt. Lasers Eng.*, vol. 95, pp. 17–25, Aug. 2017.

[5] P. Poozesh, J. Baqersad, C. Niezrecki, P. Avitabile, E. Harvey, and R. Yarala, "Large-area photogrammetry based testing of wind turbine blades," *Mech. Syst. Signal Process.*, vol. 86, pp. 98–115, Mar. 2017.

[6] J. J. Lee and M. Shinozuka, "A vision-based system for remote sensing of bridge displacement," *NDT E Int.*, vol. 39, no. 5, pp. 425–431, Jul. 2006.

[7] J. Sladek, K. Ostrowska, P. Kohut, K. Holak, A. Gaska, and T. Uhl, "Development of a vision based deflection measurement system and its accuracy assessment," *Measurement*, vol. 46, no. 3, pp. 1237–1249, Apr. 2013.

[8] Y. Fukuda, M. Q. Feng, and M. Shinozuka, "Cost-effective vision-based system for monitoring dynamic response of civil engineering structures," *Struct. Control Health Monitor.*, vol. 17, no. 8, pp. 918–936, Dec. 2010.

[9] D. Feng, M. Feng, E. Ozer, and Y. Fukuda, "A vision-based sensor for noncontact structural displacement measurement," *Sensors*, vol. 15, no. 7, pp. 16557–16575, Jun. 2015.

[10] Y. Fukuda, M. Q. Feng, Y. Narita, S. Kaneko, and T. Tanaka, "Vision-based displacement sensor for monitoring dynamic response using robust object search algorithm," *IEEE Sensors J.*, vol. 13, no. 12, pp. 4725–4732, Dec. 2013.

[11] D. Ribeiro, R. Calcada, J. Ferreira, and T. Martins, "Non-contact measurement of the dynamic displacement of railway bridges using an advanced video-based system," *Eng. Struct.*, vol. 75, pp. 164–180, Sep. 2014.

[12] Y. F. Ji and Q. W. Zhang, "A novel image-based approach for structural displacement measurement," in *Proc. Bridge Maintenance, Saf., Manage., Resilience Sustainability (IABMAS)*, 2012, pp. 407–414.

[13] G. Busca, A. Cigada, P. Mazzoleni, and E. Zappa, "Vibration monitoring of multiple bridge points by means of a unique vision-based measuring system," *Experim. Mech.*, vol. 54, pp. 255–271, Feb. 2014.

[14] M. Guizar-Sicairos, S. T. Thurman, and J. R. Fienup, "Efficient subpixel image registration algorithms," *Opt. Lett.*, vol. 33, no. 2, p. 156, Jan. 2008.

[15] B. Liu, D. Zhang, J. Guo, and C. Zhu, "Vision-based displacement measurement sensor using modified Taylor approximation approach," *Opt. Eng.*, vol. 55, no. 11, Nov. 2016, Art. no. 114103.

[16] M. Abdullah, N. Bidin, G. Krishnan, M. F. S. Ahmad, and M. Yasin, "Fiber optic radial displacement sensor-based a beam-through technique," *IEEE Sensors J.*, vol. 16, no. 2, pp. 306–311, Jan. 2016.

[17] M. Q. Feng, Y. Fukuda, D. Feng, and M. Mizuta, "Nontarget vision sensor for remote measurement of bridge dynamic response," *J. Bridge Eng.*, vol. 20, no. 12, Dec. 2015, Art. no. 04015023.

[18] N. Wadhwa, M. Rubinstein, F. Durand, and W. T. Freeman, "Phase-based video motion processing," *ACM Trans. Graph.*, vol. 32, no. 4, pp. 1–10, Jul. 2013.

[19] W. T. Freeman and E. H. Adelson, "The design and use of steerable filters," *IEEE Trans. Pattern Anal. Mach. Intell.*, vol. 13, no. 9, pp. 891–906, 1991.

[20] D. S. Reddy, S. Varadarajan, and M. N. GiriPrasad, "2D dual-tree complex wavelet transform based image analysis," *Contemp. Eng. Sci.*, vol. 5, no. 3, pp. 127–136, 2012.

[21] R. Breezer, *A First Course in Linear Algebra*. Birmingham, AL , USA: Congruent Press, 2012.

[22] R. F. Lyon, "A brief history of 'pixel,'" *Proc. SPIE*, vol. 6069, Feb. 2006, Art. no. 606901.

[23] A. Nazar, Z. M., and F. A., "Frequency estimation of single-tone sinusoids under additive and phase noise," *Int. J. Adv. Comput. Sci. Appl.*, vol. 5, no. 9, pp. 101–106, Sep. 2014.

[24] J. Baqersad, P. Poozesh, C. Niezrecki, and P. Avitabile, "Photogrammetry and optical methods in structural dynamics—A review," *Mech. Syst. Signal Process.*, vol. 86, pp. 17–34, Mar. 2017.

Matthew Southwick received the B.S. degree in mechanical engineering from the University of Pittsburgh, Pittsburgh, PA, USA, in 2019. He is currently pursuing the Ph.D. degree in mechanical engineering with the University of Massachusetts Lowell, Lowell, MA, USA. His research interest includes the development of subtle motion measurement techniques for remote sensing.

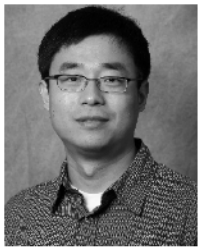

Zhu Mao received the B.S. degree in automotive engineering from Tsinghua University, Beijing, China, in 2002, and the M.S. and Ph.D. degrees in structural engineering from the University of California at San Diego, La Jolla, CA, USA, in 2008 and 2012, respectively.

He is currently with the Faculty of Department of Mechanical Engineering, University of Massachusetts Lowell, Lowell, MA, USA. He has published over 60 articles in journals and conference proceedings. He is the author of one book chapter. His research interests include structural dynamics and health monitoring, noncontact sensing and image processing, and uncertainty quantification.

Dr. Mao is a member of the American Society of Mechanical Engineers (ASME), the Society for Experimental Mechanics (SEM), and the International Society for Optics and Photonic (SPIE). He is the winner of the D. J. DeMichele Scholarship Award from SEM in 2011. He was a recipient of the Young Investigator Award from the U.S. Air Force Office of Scientific Research in 2018 and the SAGE Publishing Young Engineer Lecture Award from SEM in 2019.

Christopher Niezrecki received the dual B.S. degrees in mechanical and electrical engineering from the University of Connecticut, Storrs, CT, USA, in 1991, and the M.S. and Ph.D. degrees in mechanical engineering from the Virginia Polytechnic Institute and State University, Blacksburg, VA, USA, in 1992 and 1999, respectively.

He is currently a Professor and the Chair of the Department of Mechanical Engineering, University of Massachusetts Lowell (UMass Lowell), Lowell, USA. He is the Co-Director of the Structural Dynamics and Acoustic Systems Laboratory and leads the Center for Wind Energy at UMass Lowell. He is also the Director of the NSF-Industry/University Cooperative Research Center for Wind Energy Science Technology and Research (WindSTAR). He has been directly involved in vibrations, acoustics, smart structures, controls, and renewable energy research for over 27 years, with more than 180 publications. His areas of current research include renewable energy systems, wind turbine dynamics, monitoring, and inspection, structural dynamic and acoustic systems, smart structures, signal processing, structural health monitoring, optical sensing, and smart materials. Over the last several years, his research has focused on using optical digital image correlation for non-contacting inspection and vibration measurement of wind turbine blades/rotating structures.

Dr. Niezrecki is a member of ASME, SPIE, and SEM. He was a recipient of the National Renewable Energy Laboratory (NREL/National Wind Technology Center) Research Participant Program Fellowship in 2010. He is the 2018 Roy J. Zuckerberg Endowed Leadership Chair and a 2019 Donahue Sustainability Fellow.